Available online at www.sciencedirect.com
ScienceDirect
Journal of Power Sources 161 (2006) 1208–1216
JOURNAL OF POWER SOURCES
www.elsevier.com/locate/jpowsour

Investigation of the characteristics of a compact steam reformer integrated with a water-gas shift reactor

Yong-Seog Seo *, Dong-Joo Seo, Yu-Taek Seo, Wang-Lai Yoon

Hydrogen & Fuel Cell Research Department, Korea Institute of Energy Research (KIER), 71-2, Jang-dong, Yuseong-gu, Daejeon, 305-343, Republic of Korea

Received 8 February 2006; accepted 12 May 2006
Available online 10 July 2006

Abstract

The objective of this study is to investigate numerically a compact steam methane reforming (SMR) system integrated with a water-gas shift (WGS) reactor. Separate numerical models are established for the combustion part, SMR and WGS reaction bed. The concentration of species at the exits of the SMR and WGS bed, and the temperatures in the WGS bed are in good agreement with the measured data. Heat transfer to the catalyst beds and the catalytic reactions in the SMR and WGS catalyst bed are investigated as a function of the operation parameters. The conversion of methane at the exit of the SMR catalyst bed is calculated to be 87%, and the carbon monoxide concentration at the outlet of the WGS bed is estimated to be 0.45%. The effects of the cooling heat flux at the outside wall of the system and steam-to-carbon (S/C) ratio are also examined. As the cooling heat flux increases, both the methane conversion and carbon monoxide content are reduced in the SMR bed, and the carbon monoxide conversion is improved in the WGS bed. Both methane conversion and carbon dioxide reduction increase with increasing steam-to-carbon ratio.

Keywords: Hydrogen production; Natural gas; Numerical simulation; Steam reforming; Water-gas shift reaction; Fuel cell

1. Introduction

The fuel cell is a key technology for realizing a hydrogen economy. Various types of fuel cells that are operated with hydrogen have been developed to date. For the successful commercialization of fuel cell a stable supply of low-cost hydrogen is required. Although many technologies have been developed, the production of hydrogen from natural gas is considered to be highly promising.

The author's laboratories have conducted studies directed at the development of fuel cells and hydrogen production with an emphasis on polymer electrolyte membrane fuel cells (PEMFCs) and a system for producing hydrogen from natural gas. The PEMFC-based cogeneration systems show considerable promise for application in a small-scale distributed power generation in households. The PEMFC stack is integrated with a hydrogen-generation system to provide hot water and electricity. High efficiency, low noise, and low emission of air pollutants constitute the major benefits derived from the use of a PEMFC system [1]. To achieve this purpose, a small-scale hydrogen generation system is needed, and to address this issue, we have developed a compact steam methane reformer using natural gas as the feedstock.

Many types of fuel-processing system for producing hydrogen that is sufficiently pure and rapid for supplying a PEMFC are currently being developed [2–4]. Although the steam-reforming process requires more start-up time to reach a steady-state than an autothermal process, it can yield hydrogen concentrations above 75% in the dry product gas, while the autothermal process produces gas containing less than 50% hydrogen because of the high nitrogen content that is supplied for the internal combustion of natural gas and air [5]. Therefore, a natural gas fuel processor in which a steam-reforming process is adopted has been widely developed as one of the key components of the residential PEMFC system.

The present study focuses on developing a compact fuel-processing system for a PEMFC of 1.0 kW capacity. The unit processes of a gas burner, a steam methane reforming (SMR) reactor, a water-gas shift (WGS) reactor and internal heat exchangers are integrated into a single modular unit. Laboratory

* Corresponding author. Tel.: +82 42 860 3612; fax: +82 42 860 3134.
E-mail address: ysseo@kier.re.kr (Y.-S. Seo).

0378-7753/$ – see front matter © 2006 Elsevier B.V. All rights reserved.
doi:10.1016/j.jpowsour.2006.05.039

Nomenclature

D_p	Diameter of catalyst particle [m]
E	Total energy [J]
$\vec{g}$	Gravitational force [m s^{-2}]
h_i	Enthalpy of species i [J kg^{-1}]
J_i	Diffusion flux of species i [kg m^{-2} s^{-1}]
k	Thermal conductivity [w m^{-1} K^{-1}],
k_{eff}	Effective thermal conductivity [w m^{-1} K^{-1}]
k_f	Thermal conductivity of fluid [w m^{-1} K^{-1}]
k_s	Thermal conductivity of solid [w m^{-1} K^{-1}]
k_1, k_2, k_3	Reaction rate constants [see Table 1]
K_i	Constants [see Table 1]
m_i	Mass fraction of species i
m_p	Mass fraction of product species p
m_R	Mass fraction of reactant species R
p	Pressure [N m^{-2}]
p_i	Partial pressure of species i [bar]
R	Universal gas constant [8.314 J mol^{-1} K^{-1}]
R_i	Gas reaction rate of species i [mol m^{-3} s^{-1}]
T	Temperature [K]
$\vec{u}$	Velocity [m s^{-1}]
W_i	Molecular weight of species i [kg]
Y_i	Mole fraction of species i
ε	Dissipation rate of turbulent kinetic energy
ϕ	Porosity
η_i	Effectiveness of species i
κ	Turbulent kinetic energy
ν'	Stoichiometric coefficient for reactant
ν''	Stoichiometric coefficient for product
ρ	Density [kg m^{-3}]
τ	Stress tensor

Table 1
Parameters for kinetic model for methane steam reforming

	Pre-exponential factor (A_i) [dimension of k]	Activation energy (E_i) [kJ mol^{-1}]
Reaction rate constants for Arrhenius expression: $k_i = A_i \exp(-E_i/RT)$		
k_1 [kmol bar$^{0.5}$ kg cat^{-1} h^{-1}]	4.225×10^{15}	240.1
k_2 [kmol bar^{-1} kg cat^{-1} h^{-1}]	1.955×10^{6}	67.13
k_3 [(kml bar$^{0.5}$ kg cat^{-1} h^{-1})]	1.020×10^{15}	243.9

	Pre-exponential factor (B_i) [dimension of K]	Enthalpy change of adsorption (ΔH_i) [kJ mol^{-1}]
Constants for Van't Hoff equation: $K_i = B_i \exp(-\Delta H_i/RT)$		
K_{CO} [bar^{-1}]	8.23×10^{-5}	−70.61
K_{H_2} [bar^{-1}]	6.12×10^{-9}	−82.90
K_{CH_4} [bar^{-1}]	6.65×10^{-4}	−38.28
K_{H_2O}	1.77×10^{5}	88.68

testing is performed to investigate the characteristics of the unit and to improve its performance further.

A numerical simulation is a very useful tool for developing an efficient SMR system. Using numerical simulation, the effects of design and operating parameters can be investigated at a low cost and the results can provide basic data for designing and experimentally testing such systems. In this study, the SMR system is numerically investigated with respect to heat transfer between the heat source and the reacting catalyst bed, the reactions in the SMR and WGS catalyst beds, the effects of operating conditions, etc. To accomplish this, a numerical model applicable to the reforming system is established and the models are validated by comparing numerical results with experimental data. After validation, the reforming system is analyzed with respect to the various effects of operation and design parameters on heat transfer performance and catalytic reaction.

2. Numerical models

The numerical simulation for the SMR system is carried out by separating it into three different parts, based on its structure (see Fig. 1). One part corresponds to the heat supply which is comprised of a gas burner, a combustion chamber and a channel for the combustion gas. The second part is the SMR reaction region of the feedstock, which contains reforming catalysts. The third represents a WGS reactor that comprises a high-temperature shift (HTS) reactor (300–400 °C) and a low-temperature shift (LTS) reactor (200–300 °C). A separate numerical model was established for each part. The following describes each of the numerical models in detail.

2.1. Model of combustion and heat transfer

The numerical models described here include the modelling of combustion in the combustion chamber and heat transfer associated with the combustion gas. The computational domain was set up as an axisymmetric system that reflects the fact that the reforming system has a cylindrical shape. The governing equations for heat generation and heat transfer can be written as follows.

Continuity equation:

$$\nabla \cdot (\rho \vec{u}) = 0 \quad (1)$$

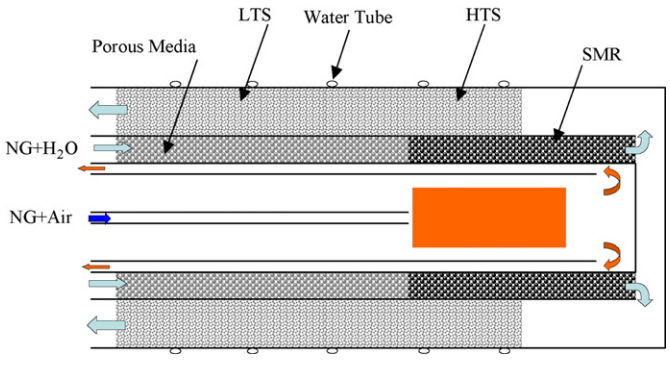

Fig. 1. Schematic of compact SMR system incorporated with WGS reactor.

Momentum equation:

$$\nabla \cdot (\rho \vec{u}\vec{u}) = -\nabla p + \nabla \vec{\vec{\tau}} + \rho \vec{g} \tag{2}$$

Energy equation:

$$\nabla \cdot (\vec{u}(\rho E + p)) = \nabla \cdot (k_{\text{eff}} \nabla T + \sum h_i \vec{J}_i + (\vec{u} \cdot \tau_{\text{eff}})) + \sum h_i R_i + \nabla \cdot \vec{q}_{\text{rad}} \tag{3}$$

Species equation:

$$\nabla \cdot (\rho \vec{u}\, m_i) = -\nabla \cdot \vec{J}_i + R_i \tag{4}$$

State equation:

$$p = \rho RT \sum \frac{Y_i}{W_i} \tag{5}$$

In the above governing equations, turbulent flow is modelled using the RNG-based κ–ε two-equation model. Details of the RNG model can be found in the literature [6]. The RNG κ–ε model is known to be more accurate and reliable than the standard κ–ε turbulent models for a wide class of flows. The combustion in the gas burner is modelled using the finite-chemistry reaction model and the eddy-dissipation model (EDM) [7]. Most fuels that are used in gas combustion are fast burning, and the overall rate of such reactions can be assumed to be controlled by turbulent mixing. In such a pre-mixed flame, as in the present study, the turbulence slowly mixes cold reactants and hot products into the reaction zone, in which the reaction starts to occur rapidly. In such a situation, the combustion is said to be mixing-limited, and the complex chemical kinetic rate can be safely neglected. Thus, the use of the eddy-dissipation model provides the advantage of a computationally low cost approach. This model calculates the net production rate with the smaller of the two following equations:

$$R_i = \nu_i' W_i A \rho \frac{\varepsilon}{\kappa} \min\left(\frac{m_{\text{R}}}{\nu_{\text{R}}' W_{\text{R}}}\right) \tag{6}$$

$$R_i = \nu_i' W_i A B \rho \frac{\varepsilon}{\kappa} \frac{\sum m_{\text{P}}}{\sum_i^N \nu_i'' W_i} \tag{7}$$

where A and B are empirical constants with values of 4.0 and 0.5, respectively.

The flame produced by gas combustion maintains a very high temperature, over 1000 °C, where radiation becomes a significant factor in heat transfer. The combustion gas participates in the radiation process, that is, it absorbs, emits and scatters radiation energy. Such a situation requires modelling of the radiative heat transfer for the combustion gas. The present study employs the discrete transfer radiation model (DTRM) [8,9] for the radiative heat transfer of the combustion gas.

In calculating the radiation of combustion gas, the selection of the appropriate radiative thermal properties, one of which is the absorption coefficient of the combustion gas, is an important issue. The present modelling uses the weighted-sum-of-grey-gases-model (WSGGM) for the absorption coefficient of the combustion gas. The WSGGM is regarded to be a quite reasonable model in combustion applications and detailed explanations can be found in the literature [10,11].

2.2. Model of SMR reaction

The SMR catalyst bed is modelled as a porous media, which reflects the fact that a reactor is packed with spherical catalysts of diameters less than 5 mm. Homogeneity is assumed in calculating the energy equation for the SMR catalyst bed. The homogeneous model assumes that the temperatures of the catalysts are the same as those of the fluid around the catalysts. The governing equations for the SMR catalyst bed can be written as follows:

Continuity equation:

$$\nabla \cdot (\rho \vec{u}) = 0 \tag{8}$$

Momentum equation:

$$\nabla \cdot (\rho \vec{u}\vec{u}) = -\nabla p + \nabla \vec{\vec{\tau}} - \frac{150}{D_{\text{p}}^2} \frac{(1-\phi)^2}{\phi^3} \cdot \mu \vec{u} \tag{9}$$

Energy equation:

$$\nabla \cdot (\vec{u}(\rho E + p)) = \nabla \cdot (k_{\text{eff}} \nabla T + \sum h_i \vec{J}_i + (\vec{u} \cdot \tau_{\text{eff}})) + \sum h_i \eta_i R_i \tag{10}$$

where $k_{\text{eff}} = \phi\, \kappa_{\text{f}} + (1+\phi)\kappa_{\text{s}}$

Species equation:

$$\nabla \cdot (\rho \vec{u}\, m_i) = -\nabla \cdot \vec{J}_i + \eta_i R_i \tag{11}$$

State equation:

$$p = \rho RT \sum \frac{Y_i}{W_i} \tag{12}$$

The above energy and species equations require the calculation of the SMR reaction in the catalyst bed. The SMR reaction can be expressed by the following equations:

$$\text{CH}_4 + \text{H}_2\text{O} \leftrightarrow \text{CO} + 3\text{H}_2 \qquad \Delta \text{H}_{298}^{\circ} = 206\ \text{kJ mol}^{-1} \tag{13}$$

$$\text{CO} + \text{H}_2\text{O} \leftrightarrow \text{CO}_2 + \text{H}_2 \qquad \Delta \text{H}_{298}^{\circ} = -41.1\ \text{kJ mol}^{-1} \tag{14}$$

$$\text{CH}_4 + 2\text{H}_2\text{O} \leftrightarrow \text{CO}_2 + 4\text{H}_2 \qquad \Delta \text{H}_{298}^{\circ} = 164.9\ \text{kJ mol}^{-1} \tag{15}$$

The kinetics of the SMR reaction have been studied by several researchers [12–14]. Xu and Froment's results [12] are employed in the present study. The intrinsic rate equations proposed by these authors are as follows:

$$r_1 = \frac{k_1}{p_{\text{H}_2}^{2.5}} \frac{(p_{\text{CH}_4} p_{\text{H}_2\text{O}} - p_{\text{H}_2}^3 p_{\text{CO}} / K_1)}{(\text{DEN})^2} \tag{16}$$

$$r_2 = \frac{k_2}{p_{H_2}} \frac{(p_{CO} p_{H_2O} - p_{H_2} p_{CO_2}/K_2)}{(DEN)^2} \quad (17)$$

$$r_3 = \frac{k_3}{p_{H_2}^{3.5}} \frac{(p_{CH_4} p_{H_2O}^2 - p_{H_2}^4 p_{CO_2}/K_3)}{(DEN)^2} \quad (18)$$

with the denominator:

$$DEN = 1 + K_{CO} p_{CO} + K_{H_2} p_{H_2} + K_{CH_4} p_{CH_4} + \frac{K_{H_2O} p_{H_2O}}{p_{H_2}} \quad (19)$$

The activation energies and pre-exponential factors for the reaction rate constants k_1, k_2 and k_3, the adsorption enthalpy change and pre-exponential factors for the adsorption constants K_{CO}, K_{H_2}, K_{CH_4} and K_{H_2O} are listed in Table 1.

For calculating the reforming reaction in the SMR catalyst bed, the effectiveness factor, η, in the above Eqs. (10) and (11) is a significant parameter. The present model uses the assumption of homogeneity between fluid and catalysts, and the effectiveness factor is not calculated separately, but is selected as 0.05 on the basis of effectiveness analyses carried out by others [15,16].

2.3. Model of WGS reaction

The WGS catalyst bed is a porous media, the same as the previous SMR reforming catalyst bed. Therefore, the governing equations for the WGS catalyst bed are the same as those for the SMR catalyst bed except for the kinetics of the WGS reaction. In general, the WGS catalyst bed consists of two operation zones, an HTS bed operated at 300–400 °C and an LTS bed operated at 200–300 °C. Fe_3O_4/Cr_2O_3 and $Cu/ZnO/Al_2O_3$ are typically used as catalysts for the high-and low-temperature bed, respectively. The present calculation uses the same kinetics for the HTS and LTS beds for ease of calculation.

The WGS reaction of the CO component can be expressed by the following equation.

$$CO + H_2O \leftrightarrow CO_2 + H_2 \qquad \Delta H^\circ_{298} = -41.1\ \text{kJ mol}^{-1} \quad (20)$$

The kinetics have been studied by several researchers [17–21]. Moe's results [20] are employed in the present study, the rate equation is as follows:

$$r_4 = k_4\, p_{CO}\, p_{H_2O} \left(1 - \frac{p_{H_2} p_{CO_2}}{K_2 p_{CO} p_{H_2O}}\right) \quad (21)$$

$$k_4 = 1.85 \times 10^{-5} \exp\left(12.88 - \frac{1855.5}{T}\right) [\text{mol g}^{-1}\ \text{min}^{-1}] \quad (22)$$

To solve the complete set of governing equations established for gas combustion, the SMR reaction and the WGS reaction, the FLUENT software program [22] is used. Since three parts of gas combustion, SMR and WGS reactions, are coupled with each other, their governing equations are solved simultaneously. To ensure the accuracy of the calculation, however, each part is tested individually before coupling. The results of the numerical calculation are compared with experimental data in order to validate the models.

3. Results and discussion

3.1. Characteristics of combustor, SMR and WGS reactor

The SMR reaction is a highly intensive endothermic process. The heat required for the reforming reaction is supplied by the combustion gas via a gas burner. A schematic of the SMR system integrated with a WGS reactor is shown in Fig. 1. For effective heat transfer from the combustion gas to the SMR catalyst bed, a narrow flow channel is placed next to the SMR catalyst bed. The combustion gas supplies the main heat energy to the SMR catalyst bed during its passage through the channel. A mixture of natural gas (CH_4) and steam, as a feedstock, is fed to the SMR catalyst bed, which absorbs the heat energy from the combustion gas. Before the feedstock reaches the SMR catalyst, it passes through porous media, which fills the channel to produce a uniform flow of feedstock and also to enhance the heat transfer from the combustion gas to the feedstock. The feedstock in the SMR catalyst is converted into reformed gas, which then flows into the WGS catalyst bed (HTS + LTS), located in the outermost channel of the system. The WGS bed reduces the carbon monoxide content of the reformed gas to less than 1.0%. The WGS reaction generates a slight amount of heat and must be cooled. To accomplish this, cooling water tubes are installed around the WGS bed. The cooling water in the tubes is converted into steam by the heat transfer and is used as the feedstock of the SMR.

To check the validity of the numerical simulation, the calculated results were compared with experimental data. Fig. 2 illustrates a comparison between the experimental and calculated on temperatures of the WGS catalyst bed. The calculated temperatures show slightly lower values in the inlet of the WGS

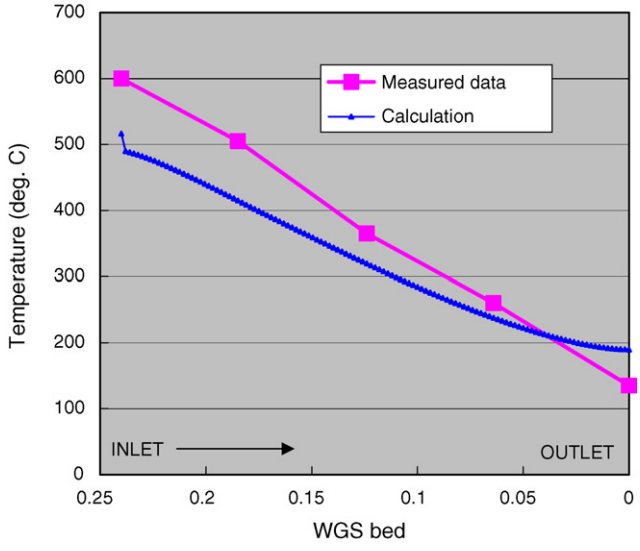

Fig. 2. Comparison of calculated and measured temperatures along centerline of WGS bed.

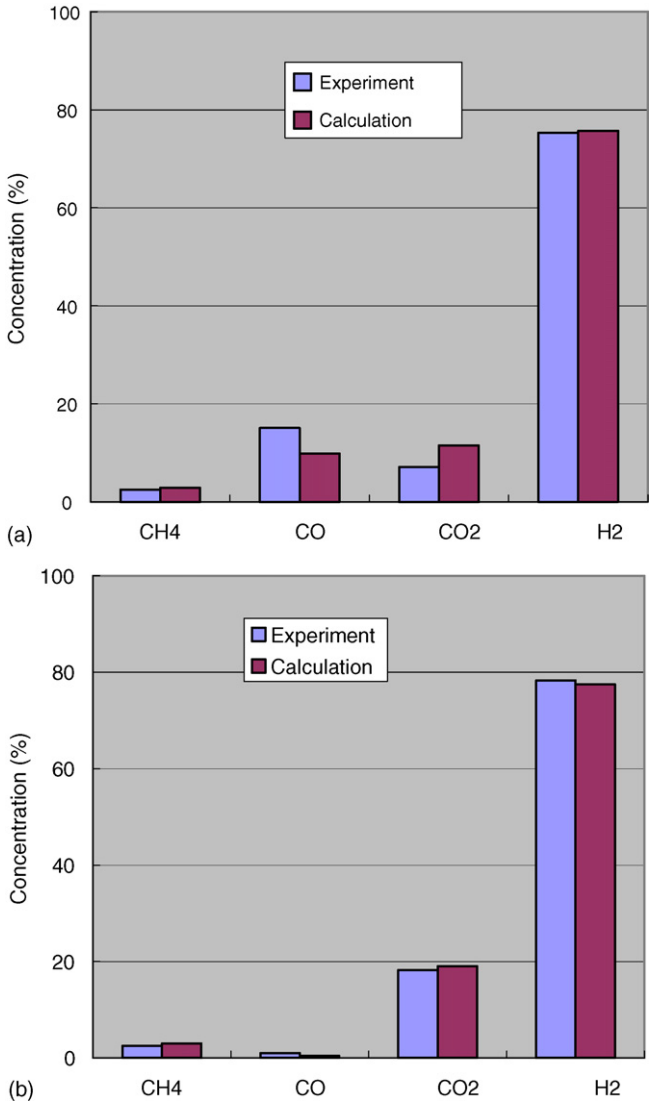

Fig. 3. Comparison of calculation and measured data on species at (a) exit of SMR catalyst bed and (b) WGS catalyst bed.

bed and are slightly higher in the exit than the measured data. A comparison of the products in the SMR and WGS catalyst bed is shown in Fig. 3. The calculated values for CH_4 and H_2 are very close to the experimental data, while the carbon monoxide and CO_2 contents deviate slightly from the measured data. Such a difference may be caused by an inaccurate calculation of reaction rate or any other reason. Even though some discrepancy exists in the calculation results, the numerical simulation would be expected to provide a useful tool for analyzing the effects of various design and operation parameters.

Heat transfer from the combustion gas to the SMR and WGS catalyst bed was investigated. Fig. 4 illustrates the temperature distribution in the combustor and the catalyst beds of SMR and WGS. Within the combustor, the highest temperature is along the central line of the combustor, which could alleviate the risk of hot spots on the wall of the SMR catalyst bed. Nevertheless, the top end of the combustor reaches a very high temperature and should be made of sufficiently strong steel plate. The combustion gas passes through the channel between the combustor and the SMR

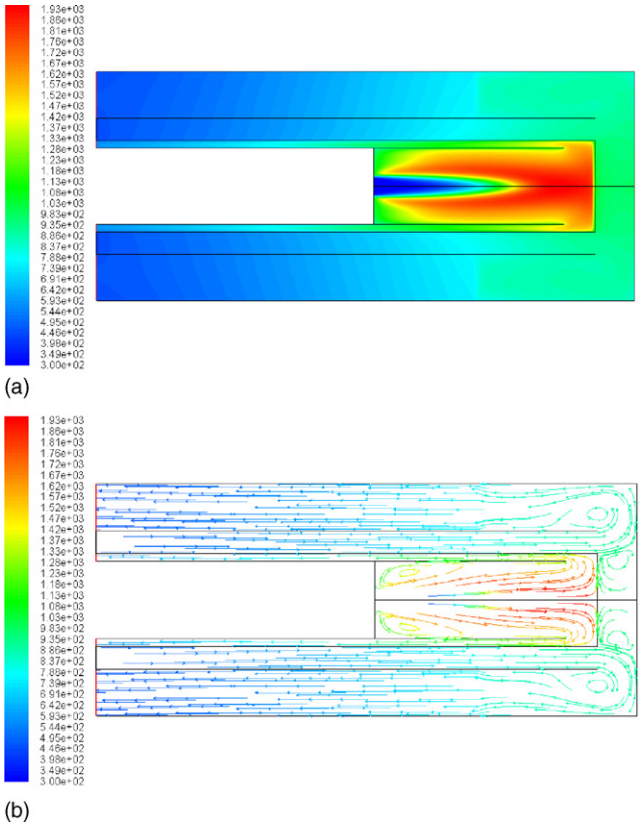

Fig. 4. (a) Temperature and (b) path line distribution in SMR system.

catalyst, and the heat is transferred from the combustion gas into the SMR bed for methane steam reforming, an endothermic reaction.

Fig. 5 describes the temperature profile of the combustion gas, in the channels of the SMR and WGS bed. In the channel for the combustion gas, the temperature drops rapidly from about 1100 °C to below 320 °C along the flow of combustion gas. This is due to heat transfer from the combustion gas to the SMR catalyst bed. The temperature in the SMR catalyst bed next to the channel for the combustion gas increases linearly from about

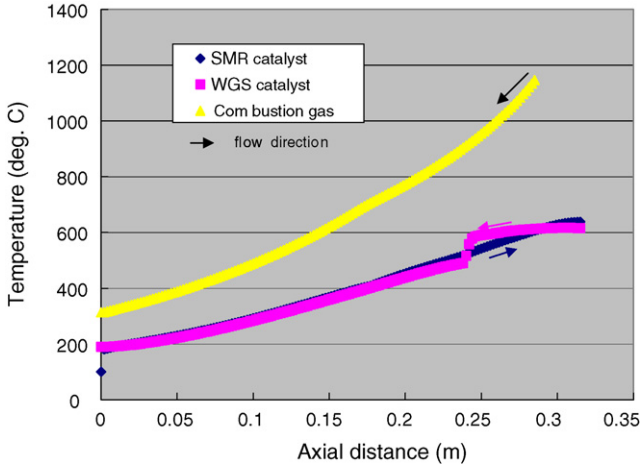

Fig. 5. Temperature profiles along combustion gas channel, SMR and WGS catalyst bed.

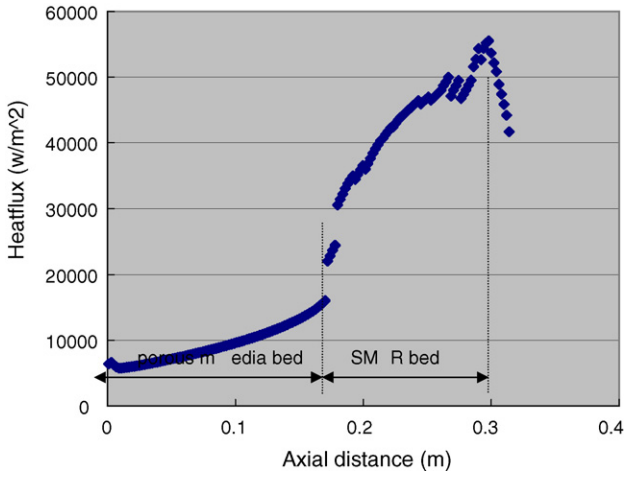

Fig. 6. Heat flux profiles from combustion gas to SMR catalyst bed.

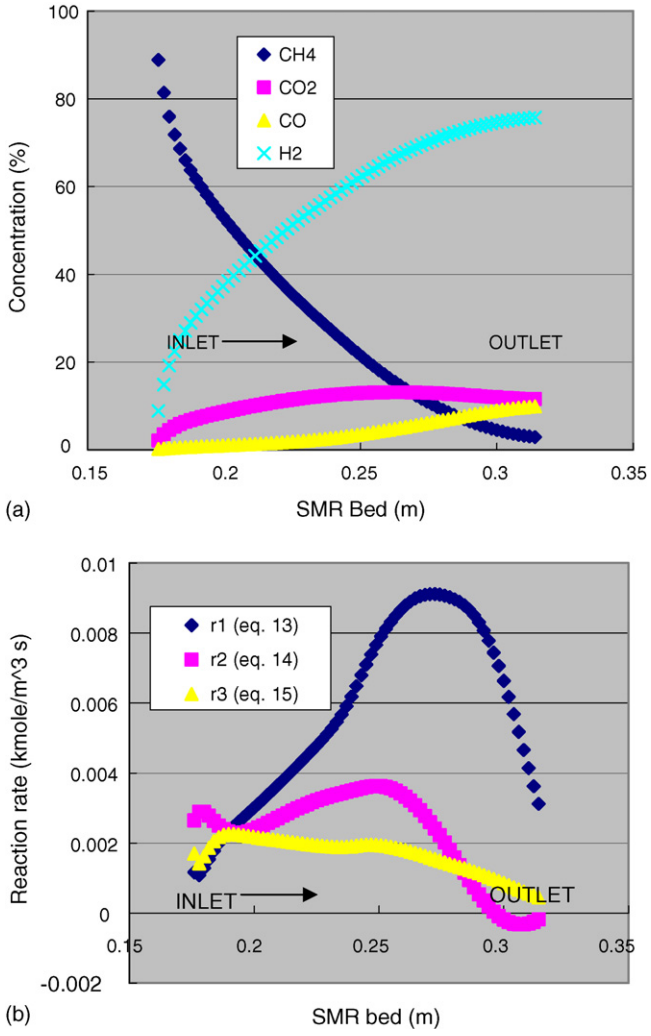

Fig. 7. (a) Profiles of gas components and (b) reaction rate in SMR catalyst bed.

100 °C to around 640 °C. The temperature in the WGS channel decreases steadily from 616 °C at the inlet to 190 °C at the outlet. Such a decrease in the temperature of the WGS bed is caused by the cooling water tubes installed around the WGS channel. The computed data show that temperatures in the channel for the combustion gas are by 100–250 °C higher than those in the SMR bed, but the temperatures in the SMR bed are nearly the same as those in the WGS bed. The reason for this is that the SMR bed and the WGS bed are filled with catalysts, which act as media to augment heat transfer. Similarly if any porous medium is installed in the channel for the combustion gas, it will improve the heat transfer to the SMR bed from the combustion gas.

Fig. 6 shows the heat flux on to the wall of the SMR catalyst bed. The heat flux is in the range 5.7–16.0 kW m^{-2} in the region of the porous media and 16.0–55.2 kW m^{-2} in the region of the SMR catalyst. The amount of heat transferred from the combustion gas is calculated to be 3.08 kW in the porous media and 10.46 kW in the SMR catalyst. The total heat transferred from the combustion gas to the SMR channel is 13.54 kW, which is estimated to be 76.1% of the total heat energy supplied from the gas burner. The residual heat contained in the flue gas can be recovered through additional heat exchangers (not shown in Fig. 1.) Achieving a high thermal efficiency is an important target in developing a new compact reformer system. The higher heat recovery from the combustion gas leads to a more efficient reformer system in terms of thermal energy. The analysis suggests that it would be desirable to enhance further heat transfer from the combustion gas to the SMR channel.

The concentration profiles of species within the SMR catalyst bed are depicted in Fig. 7(a). The CH_4 concentration decreases rapidly from the inlet of the SMR catalyst and reduces to its lowest level (2.8%) at the outlet of the catalyst bed. The H_2 concentration rapidly increases from the inlet and reaches a peak near the outlet. The profile for H_2 concentration is inversely analogous to the CH_4 concentration profile. By contrast, pattern for the CO concentration profile is slightly different from that for H_2. The CO concentration in the front part of the SMR bed increases more slowly than in the rear part of the SMR bed. On the other hand, Fig. 7(b) represents the reaction rate for each of the reaction process, r1, r2 and r3 in Eqs. (13)–(15). The data reveal that the r1 reaction is the dominant process among the three reaction processes. Its rate increases from the inlet of the SMR bed and reaches the maximum after the middle of the bed, then decreases rapidly. The r2 reaction shows a backward reaction near the exit of the bed, depicted as a negative reaction rate. The r2 reaction is a mild exothermic reaction and the equilibrium constant decreases with increasing temperature. As described above, the temperature in the SMR bed increases along the flow of reactants. The r2 reaction reaches a peak around the middle of the catalyst bed, then decreases steadily, and eventually reaches a negative value.

The reformed gas exiting from the SMR catalyst bed is then fed to the WGS catalyst bed, where the CO is reduced via the WGS reaction (Eq. (20)). Fig. 8 represents the species profiles and the WGS reaction rate. The CO decreases rapidly from 8.7% at the inlet to 0.5% at the outlet, while the CO_2 increases from 12.5 to 19.1% through the WGS bed. The CH_4 concentration shows little change through the catalyst bed. Fig. 8(b) shows a plot of the reaction rate of Eq. (20) in the WGS bed. The reaction rate decreases drastically near the inlet and then slowly decreases toward the outlet. The temperature in the WGS bed

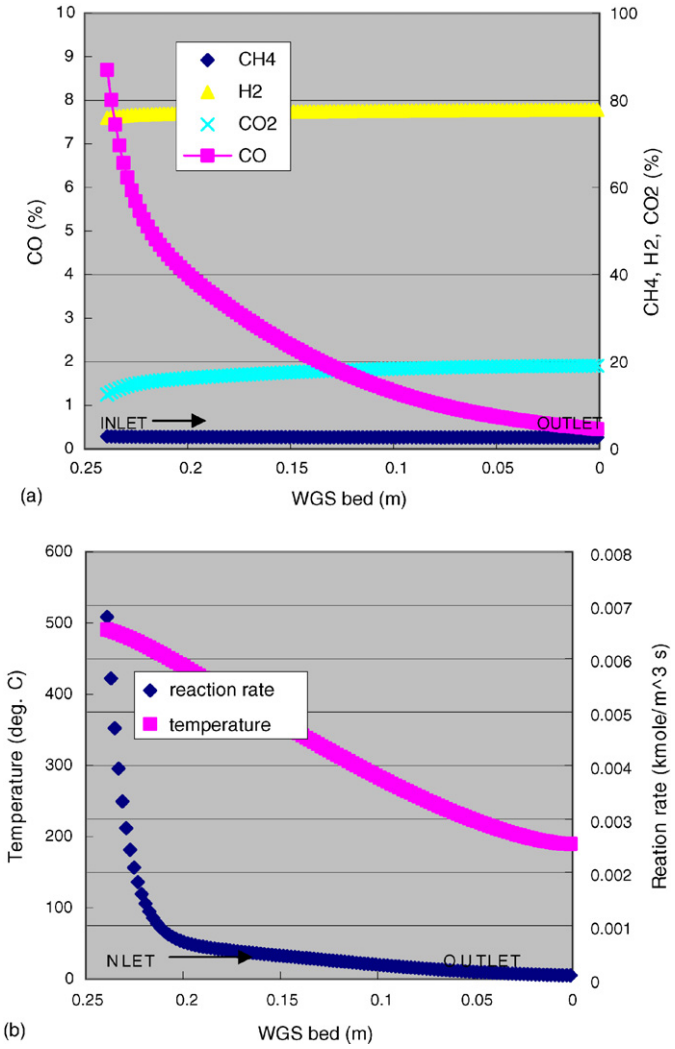

Fig. 8. (a) Profiles of species and (b) reaction rate in WGS catalyst bed.

changes from 489 °C at the inlet to 190 °C at the outlet, as the result of cooling at the outside of the WGS bed. The heat flux is set to 7000 W m^{-2} at the outside wall of the WGS bed.

3.2. *Effects of operation parameters*

For a specified SMR system, several operation parameters can significantly influence the performance of the system. One of them is thought to be a cooling heat flux at the outermost wall of the system. The cooling lowers the temperature of the WGS catalyst bed so that it operates at a low temperature for the efficient conversion of CO. As described above, the HTS is operated at temperatures of 300–400 °C and the LTS at temperatures of 200–300 °C. The amount of the cooling heat flux would be expected to affect directly not only the performance of HTS and LTS but also the performance of the SMR bed. Fig. 9 depicts the effects of a cooling heat flux on temperatures in the WGS bed. These decrease with increasing cooling heat flux. The temperatures near the exit of the WGS bed are more heavily affected by the cooling heat flux than those near its inlet. Fig. 10 shows the effects of the cooling heat flux on the reforming reaction in

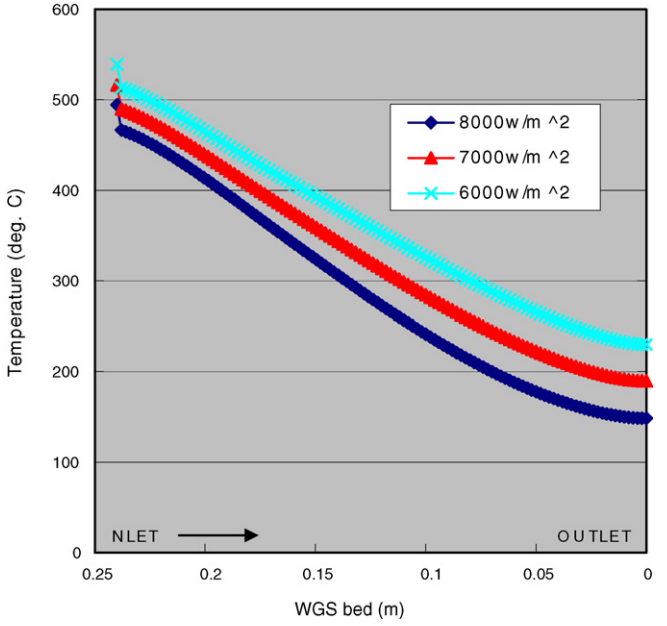

Fig. 9. Effects of cooling heat flux at outermost wall of system on temperatures in WGS bed.

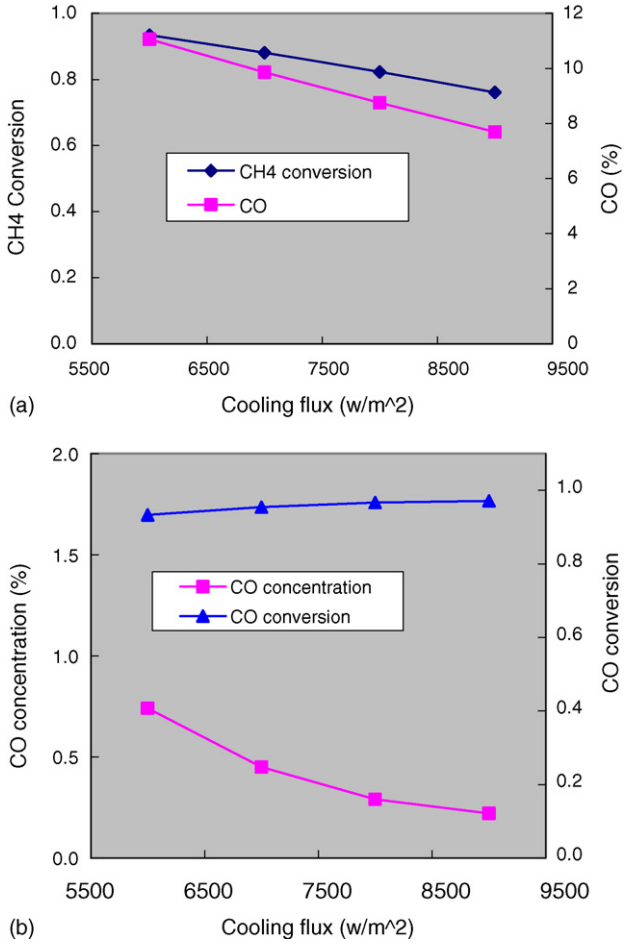

Fig. 10. (a) Species at the SMR outlet and (b) WGS outlet as function of cooling heat flux at outermost wall of system.

the SMR and on CO conversion in the WGS bed. As the cooling heat flux increases, methane conversion and the CO content in the SMR bed both decrease. The reason for the decrease in methane conversion is that the higher cooling heat flux lowers the temperature of the SMR bed, so that the reactions of Eqs. (13)–(15) move to an equilibrium corresponding to the lower temperature and thus result in a lower conversion of methane. This suggests that the cooling heat flux should be controlled appropriately so as not to drop the conversion of methane to less than the target level. As an example, the target for CH_4 conversion in the present development is over 85%, which requires the cooling heat flux to be maintained at less than 7000 W m^{-2}. An investigation concerning the CO conversion in the WGS bed reveals that it increases as the cooling heat flux is increased (see Fig. 10(b)). The CO at the outlet of the WGS bed is also reduced with increase in the cooling heat flux. This analysis suggests that the cooling heat flux should be as high as possible to reduce the CO content at the exit of the WGS bed. The maximum cooling heat flux is limited due to the target for methane conversion. In the case of the present design, it is recommended that the cooling heat flux be increased up to 7000 W m^{-2} to obtain the maximum conversion of CH_4 in the SMR bed and the maximum reduction of CO in the WGS bed.

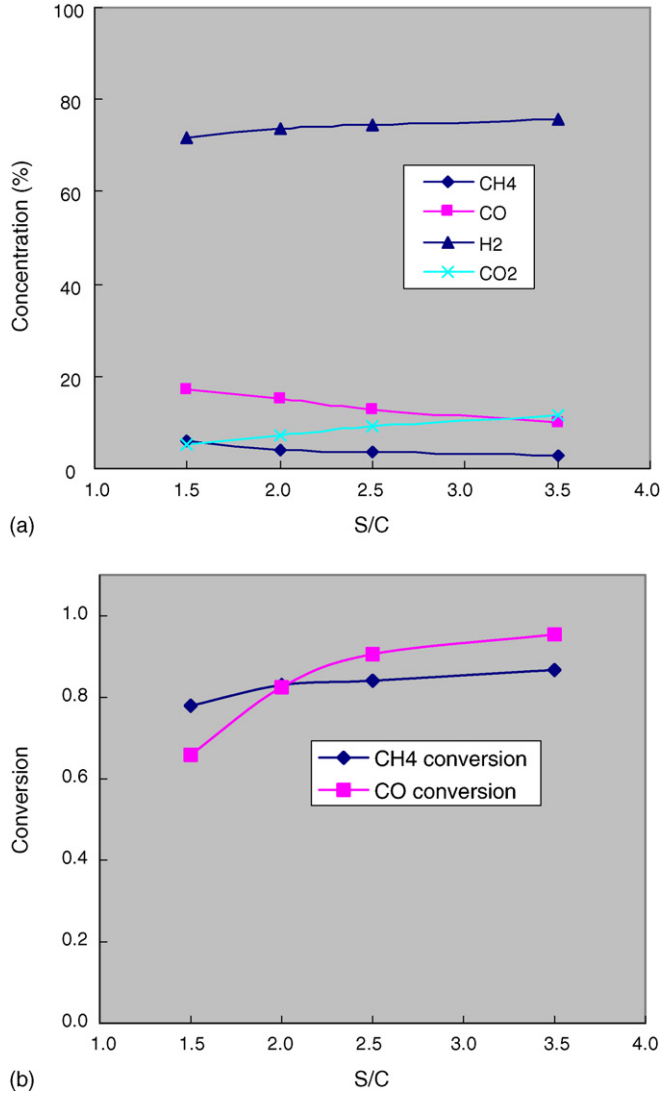

Fig. 11. Effects of S/C ratio (a) reforming reaction in SMR and (b) CO conversion in WGS bed.

Another important parameter of the reforming system is the steam-to-carbon (S/C) ratio of the feedstock. The steam content in the feedstock is very important. The theoretical value for the S/C ratio is 1.0, as shown in Eq. (13), however, in practice coking of carbon occurs in the reforming catalyst of the SMR bed. Accordingly the S/C ratio is maintained over 1.0 to avoid carbon coking and also to increase the conversion of methane. Thus, the effects of the S/C ratio on the reforming reaction in the SMR bed and on CO conversion in the WGS bed were investigated; the results are plotted in Fig. 11. The results for the SMR bed show that methane conversion increases as the S/C is increased, leading to an increase in the content of H_2 and CO_2 and a decrease in CO content. The S/C ratio also significantly affects CO conversion in the WGS bed, as shown in Fig. 11(b). As the S/C ratio increases, the CO conversion is enhanced. The calculation also shows that the degree of enhancement in CO conversion is stronger than that for methane conversion. The analysis implies that the S/C ratio should be maintained as high as possible. On the other hand, maximum supply of steam is limited within the allowable cost of steam generation. A higher S/C ratio leads to a lower thermal efficiency of the SMR system. Therefore, the S/C should be properly determined considering the relation between the increase in the conversion of methane and CO and the disadvantage in thermal efficiency.

4. Conclusions

To investigate a compact SMR system integrated with a WGS reactor, a numerical simulation has been conducted. For the numerical calculation, numerical models were first established. The present SMR system consists of three parts: a combustor, an SMR catalyst bed, and a WGS catalyst bed. Thus, the numerical model is separately set up for each part. One is a model for combustion and heat transfer, and the other two are models for the SMR and WGS reactions. The SMR and WGS catalyst beds are modelled as a porous media and are assumed to be homogeneous in calculating the energy equation. After establishing the models, the calculations are validated by comparing the calculation results with experimental data. The species concentration at the exit of the SMR and WGS bed and the temperatures in the WGS bed are in good agreement with the measured data.

After establishing the numerical model, the SMR system is investigated with respect to heat transfer to the catalyst beds, and catalytic reactions in the SMR and WGS catalyst bed. The amount of heat transferred to the SMR bed from the gas burner is estimated to be 76.1% of the total heat energy supplied from the combustion gas. The calculation suggests that the heat transferred to the catalyst bed should be further increased in order to enhance the thermal efficiency of the SMR system. The conversion of CH_4 at the exit of the SMR catalyst bed is calculated to be 87%, and CO at the outlet of the WGS bed is estimated to be 0.45%. It is also shown that for the r2 reaction (Eq. (14)), the

backward reaction takes place in the high-temperature region of the SMR bed.

The effects of operation parameters, such as cooling heat flux at the outside wall of the system and steam-to-carbon (S/C) ratio, have also been investigated. As the cooling heat flux increases, both CH_4 conversion and CO content are reduced in the SMR bed, and CO conversion is improved in the WGS bed. The analysis implies that the cooling heat flux can be increased to 7000 W m^{-2} while CH_4 conversion is maintained at over 85%. On the other hand, the results show that the S/C ratio has a significant influence on CH_4 conversion in the SMR and CO reduction in the WGS. As the S/C ratio is increased, CH_4 conversion and CO reduction both increase. The S/C ratio should be maintained at as high a value as possible, but the maximum supply of steam is limited within the allowable cost of steam generation.

References

[1] K. Nishizaki, M. Kawamura, N. Osaka, K. Ito, N. Fujiwara, Y. Nishizaka, H. Kitazawa, Abstracts of 2005 Fuel Cell Seminar, 2005, pp. 299–302.
[2] T. Takahasi, Y. Nishzaka, K. Ito, N. Osaka, K. Kobayashi, H. Horinouchi, R. Toriumi, T. Miura, K. Nishizaki, Abstracts of 2004 Fuel Cell Seminar (2004) 295.
[3] Y. Ikeda, T. Kiyota, A. Kabasawa, Y. Chida, Abstracts of 2004 Fuel Cell Seminar (2004).
[4] G. Gigliucci, L. Pertruzzi, E. Cerelli, A. Garzisi, A. La Mendola, J. Power Sources 131 (2004) 62–68.
[5] N. Shinke, S. Ibe, S. Takami, Y. Yasuda, H. Asatsu, M. Echigo, T. Tabata, Abstracts of 2002 Fuel Cell Seminar (2002) 956.
[6] D. Choudhury, Introduction to the Renormalization Group Method and Turbulence modeling, Fluent Inc., 1993, Technical Memorandum TM-107.
[7] B.F. Magnussen, B.H. Hjertager, Proceedings of the 16th International Symposium on Combustion, The Combustion Institute, 1976.
[8] M.G. Carvalho, T. Farias, P. Fontes, Fundamental Of Radiation Head Transfer, ASME HTD 160 (1991) 17–26.
[9] N.G. Shah, A new method of computation of radiant head transfer in combustion chambers, Ph.D. thesis, Imperial College of Science and Technology, 1979.
[10] A. Coppalle, P. Vervisch, Combustion and Flame 49 (1983) 101–108.
[11] T.F. Smith, Z.F. Shen, J.N. Friedman, J. Heat Transfer 104 (1982) 602–608.
[12] J. Xu, G.F. Froment, AIChE J. 35 (1989) 88–96.
[13] K. Hou, R. Hughes, Chem. Eng. J. 82 (2001) 311–328.
[14] T. Nugaguchi, K. Kikuchi, Chem. Eng. Sci. 43 (1988) 2295.
[15] J. Xu, G.F. Froment, AIChE J. 35 (1989) 97–103.
[16] M.N. Pedernera, J. Pina, D.O. Borio, V. Bucala, Chem. Eng. J. 94 (2003) 29–40.
[17] J. Sun, J. Desjardins, J. Buglass, K. Liu, Int. J. Hydrogen Energy 30 (2005) 1259–1264.
[18] N.E. Amadeo, M.A. Laborde, Int. J. Hydrogen Energy 20 (12) (1995) 949–956.
[19] N.A. Koryabkina, A. Phatak, W. Ruettinger, R. Farrauto, F. Riberiro, J. Catal. 217 (2003) 233–239.
[20] J.M. Moe, Chem. Eng. Prog. 58 (1962) 33.
[21] J. Gonzalez, M. Gutierrez, J. Gonzalez, N. Amadeo, M. Laborde, M. Paz, Chem. Eng. Sci. 47 (6) (1992) 1495–1501.
[22] Fluent software. FLUENT User's guide. Fluent Incorporated, http://www.fluent.com, 2005.